Macromolecules

Article

pubs.acs.org/Macromolecules

Thermo-Induced Limited Aggregation of Responsive Star Polyelectrolytes

Weinan Xu,[†] Ikjun Choi,[†] Felix A. Plamper,[§] Christopher V. Synatschke,[‡] Axel H. E. Müller,[‡,∥] Yuri B. Melnichenko,[⊥] and Vladimir V. Tsukruk[†,*]

[†]School of Materials Science and Engineering, Georgia Institute of Technology, Atlanta, Georgia 30332, United States

[‡]Makromolekulare Chemie II and Bayreuther Zentrum für Kolloide und Grenzflächen, Universität Bayreuth, D-95440 Bayreuth, Germany

[⊥]Biology and Soft Matter Science Division, Neutron Scattering Directorate, Oak Ridge National Laboratory, Oak Ridge, Tennessee 37381, United States

[§]Institute of Physical Chemistry, RWTH Aachen University, 52056 Aachen, Germany

Supporting Information

ABSTRACT: Poly(*N*,*N*-dimethylaminoethyl methacrylate) (PDMAEMA) star polyelectrolytes with dual thermo- and pH-responsive properties have been studied by *in situ* small-angle neutron scattering at different temperatures and pH conditions in order to reveal their conformational changes in semidilute solution. At pH values close to the pK_a, all PDMAEMA stars studied here are partially charged and show a core−shell quasi-micellar morphology caused by microphase separation with a collapsed core region with high monomer density and a hydrated loosely packed shell region. Upon increasing the temperature, the PDMAEMA star polyelectrolytes first experience a contraction in the shell region while the core size remains almost unchanged, and then start to form limited intermolecular aggregates. With decreasing pH values, the transition temperature increases and the size of the aggregates decreases (average aggregation number changes from 10 to 3). We suggest that these changes are triggered by the decrease in solvent quality with increasing temperature, which leads to the transition from an electrostatically dominated regime to a regime dominated by hydrophobic interactions. The observed phenomenon is in striking contrast to the phase behavior of linear PDMAEMA polyelectrolytes, which show macrophase separation with increasing temperature under the same conditions.

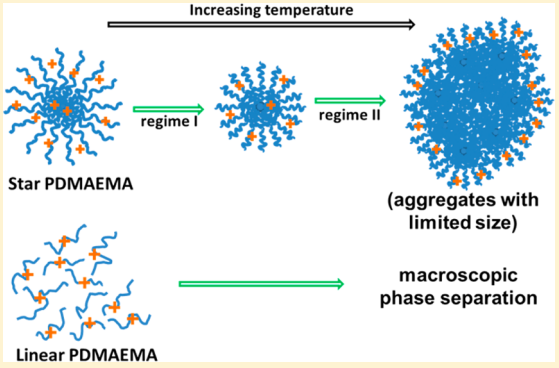

INTRODUCTION

Recent advances in polymer chemistry allow the synthesis of branched polyelectrolytes with well-defined structures, such as polyelectrolyte brushes,[1,2] dendritic polyelectrolytes,[3] hyperbranched amphiphiles and polyelectrolytes,[4,5] pearl-necklace polyelectrolytes,[6] and star amphiphilic and polyelectrolyte block-copolymers.[7−11] Among many different kinds of branched polyelectrolytes, star polyelectrolytes constitute a particular class of macromolecules with high relevance in soft matter physics, chemistry, and materials science.[12,13] Due to the unique architecture of star polyelectrolytes, their conformational state can be complicated and affected by the degree of charging, the salt concentration, the valency of counterions and co-ions, as well as the temperature and pH of the solution.[7,14,15] Star and linear polyelectrolytes frequently show peculiar phase behavior due to complex balance of intra- and intermolecular ionic interactions. For instance, the crossover from a dilute to a semidilute solution regime occurs at much lower polymer concentrations than for solutions of neutral chains.[16,17] Muthukumar et al.[18] reported a novel mechanism of phase separation upon temperature change for aqueous solutions of poly(sodium 4-styrenesulfonate) (PSS), where an enrichment of polymer aggregates of well-defined size occurs in the very early stage of nucleation, which is then followed by a growth process in the formation of the new phase. In the latter stage, the polymer aggregates formed in the early stage act as the templating nuclei with the daughter phases have different polymer charges from that of the mother phase.[19]

Theoretical studies have shown that in addition to the steric repulsion between star polymers, there are also a relatively short-range attraction and a secondary repulsive barrier at longer distance.[20] It has been demonstrated that solutions of weakly charged polyelectrolytes exhibit a microphase separation upon a decrease in the solvent quality below the Θ-point.[21] At appropriate thermodynamic conditions, the system has a tendency to form clustered regions, however, true macrophase

Received: January 20, 2014
Revised: February 24, 2014
Published: March 7, 2014

   dx.doi.org/10.1021/ma500153w | *Macromolecules* 2014, 47, 2112−2121

Scheme 1. Chemical Structure of PDMAEMA Star Polyelectrolytes (Left) and Their Quaternized Salts (Right)

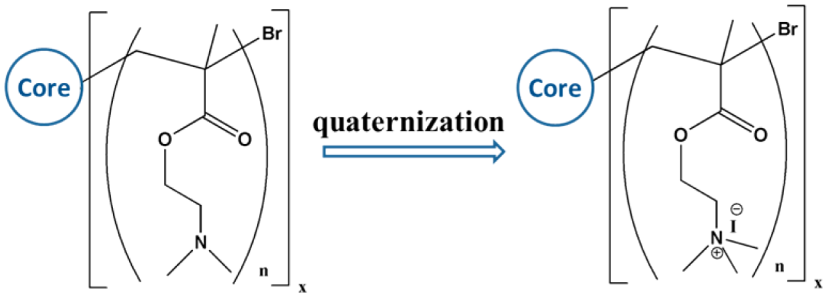

Table 1. Structural Parameters for PDMAEMA Star Polyelectrolytes and Their Quaternized Salts with Different Number of Arms or Arm Length (All Units in nm, and M_w Unit in g/mol)

sample	M_w[a]	core radius	shell thickness	overall R	R_g (Kratky)	R_g ($p(r)$)	effective radius[b]	D (peak position)[c]
$(PDMAEMA_{170})_{9.5}$	3.00×10^5	3.5 ± 0.2	3.7 ± 0.3	7.2 ± 0.5	7.5 ± 0.3	7.0 ± 0.4	11.0	37.8
$(PDMAEMA_{170})_{18}$	6.90×10^5	5.2 ± 0.2	4.8 ± 0.2	10.0 ± 0.4	10.4 ± 0.3	9.0 ± 0.5	15.2	49.9
$(PDMAEMA_{240})_{24}$	1.36×10^6	6.1 ± 0.3	6.2 ± 0.5	12.3 ± 0.8	12.8 ± 0.4	12.0 ± 0.4	23.0	65.8
$(qPDMAEMA_{170})_{9.5}$	5.76×10^5	–	–	–	10.9 ± 0.4	–	–	41.5
$(qPDMAEMA_{170})_{18}$	1.10×10^6	–	–	–	15.1 ± 0.3	–	–	56
$(qPDMAEMA_{240})_{24}$	2.21×10^6	–	–	–	17.3 ± 0.4	–	–	65.8

[a]Weight average molecular weight (M_w) determined by static light scattering (SLS) in acetone.[37] [b]The effective radius values are from MSA structure factor (Supporting Information). [c]The distance D is calculated from the peak position at low q range in Figure 1a.

separation might be inhibited. The affecting factors include counterion concentration and valency, pH, and temperature, among others. The role of temperature in the solution behavior of linear polyelectrolytes has been considered.[22] The correlation length for concentration fluctuations in aqueous solutions of PSS with added salt was determined, and the critical behavior was observed upon lowering the temperature to phase boundaries. Khokhlov et al.[23] showed that for partially charged weak polyelectrolytes the counterions can easily transfer between repeating units and from one chain to another, which facilitates the conventional phase separation in solution. A study on polyelectrolyte micelles also showed that with increasing packing fraction and minimal screening conditions, the micelle stars shrink and the corona layers eventually interdigitate, and this effect is most pronounced for higher corona charge.[24] Another study on thermo-responsive micelles also showed that the shell collapses upon heating, followed by intermicellar aggregation and densification.[25]

On the other hand, the temperature effects on the interactions and phase behavior of star polyelectrolytes have hardly received any attention. Considering recent utilization of star polyelectrolytes for building hollow microcapsules,[26,27] conformal coatings[28] with tunable properties as well as in gene delivery,[29] the elucidation of the responsive behavior of star polyelectrolytes in solution becomes important.[30] For the investigation of the temperature behavior of polyelectrolyte solution, classical macroscopic methods such as turbidimetry cannot be applied to monitor local conformational and aggregation behavior. The characteristic dimensions and internal morphology can be obtained from the neutron scattering data, which is sensitive to inner morphology if a high contrast is achieved in deuterated environment. Small-angle neutron scattering (SANS) has been used to study the thermo-responsive properties of block copolymers,[31] gels,[32] microgel colloids,[33] micelles,[34] and other related soft materials.[35] For instance, Moore et al.[36] studied the aggregation behavior of thermally responsive star block copolymers where the interior block of *N*-isopropylacrylamide (NIPAM) can collapse when heated above its low critical solution temperature (LCST).

In this paper, we discuss the solution behavior of novel star polyelectrolytes consisting of poly(*N*,*N*-dimethylaminoethyl methacrylate) (PDMAEMA) with dual-responsive properties by using *in situ* SANS measurements at different temperatures and pH values around pK_a when they are partially charged (pK_a is 5.8 for $(PDMAEMA_{170})_{18}$).[37] Since PDMAEMA is a weak polyelectrolyte, the protonation/deprotonation equilibrium depends on the pH conditions and solution temperature.[38] We observed that PDMAEMA star polyelectrolytes in semi-dilute solution form core−shell microphase separated micelles with limited short-range intermolecular ordering. Upon heating from room temperature to narrow temperature interval, within 45−50 °C, a modest contraction of brush-like shells was observed, which was induced by the reduced osmotic pressure with changes in local pH. In this temperature range, their dense collapsed cores remain almost unchanged while the arm chains in their loose shells undergo significant densification and contraction (about 50%). At even higher temperature (> 45 °C), but well below cloud point at these pH conditions (> 80 °C)[38] a limited intermolecular aggregation with aggregation number below 10 has been detected. This behavior is in striking contrast to the common macroscopic phase separation of their linear PDMAEMA counterparts studied here as well under the same conditions.

EXPERIMENTAL SECTION

Materials. PDMAEMA star polymers were synthesized by atom transfer radical polymerization of 2-(*N*,*N*-dimethylamino)ethyl methacrylate employing a core-first route with functionalized polyhedral oligomeric silsesquioxane (POSS) core (described earlier[37]). The chemical structure is shown in Scheme 1.

Sugar-based scaffolds as well as silsesquioxane nanoparticles were used as multifunctional initiators. Subsequent quaternization of the obtained PDMAEMA stars yielded their star-shaped quaternized ammonium salts (qPDMAEMA). The rather low efficiency of the

dx.doi.org/10.1021/ma500153w | Macromolecules 2014, 47, 2112−2121

initiation sites (30−75%) leads to a moderate arm number distribution of the prepared polyelectrolyte stars. Here, we used PDMAEMA star polymers with arm numbers of 9.5, 18, and 24 (number average), the number-average degree of polymerization per arm is 170, 170, and 240, respectively (Table 1). Therefore, they are named as $(PDMAEMA_{170})_{9.5}$, $(PDMAEMA_{170})_{18}$, and $(PDMAEMA_{240})_{24}$, with the number-average molecular weights of 250 000, 490 000, and 950 000 g/mol, and polydispersity indexes of 1.20, 1.41 and 1.43, respectively.

To ensure high scattering contrast, D_2O (99.9%) was used to dissolve star polyelectrolytes for SANS experiments (Cambridge Isotope Laboratories). Sodium deuteroxide (40 wt % in D_2O, 99 atom % D) and deuterium chloride (99 atom % D) were purchased from Sigma-Aldrich, and used to adjust the pH of the samples. Nanopure water (Nanopure system, Barnstead) with a resistivity of 18.2 MΩ·cm was used as well.

For DLS measurements we used a Malvern Instruments Zetasizer Nano ZS (Malvern Instruments) with a 4 mW He−Ne 633 nm laser. Measurements were performed at a detection angle of 173° (back scattering), and Malvern Zetasizer software (v6.20) was used to analyze the data. Molecular models of arm chains were built using Materials Studio with energy minimization combined with cycles of molecular dynamics.

Small Angle Neutron Scattering Experiments. SANS measurements were conducted at Oak Ridge National Laboratory (ORNL) on the CG2 (GP-SANS) instrument with a wavelength of λ = 4.7 Å ($\Delta\lambda/\lambda \sim 0.14$). Polyelectrolyte solutions were loaded into 2 mm thick quartz cells. Quartz cells were mounted in a temperature-controlled sample holder (temperature stability and gradients are better than ±0.1 °C), and the samples were allowed to stabilize for 10 min at given temperature before each measurement. Polymer concentration in our experiments was chosen to be 1 wt % in order to keep high signal-to-noise ratio and minimize possible interactions between the stars and large scale aggregate formation. Two sample−detector distances were used (1.0 and 18.5 m with a 40 cm detector offset), which resulted in a range of scattering vectors q ($q = 4\pi\cdot\sin\theta/\lambda$, where 2θ is the scattering angle) covered in the experiment from 0.004 to 0.6 $Å^{-1}$. The data were corrected for instrumental background and detector efficiency and converted to an absolute scale (cross section $I(q)$ in units of cm^{-1}) by means of a precalibrated secondary standard, Al-4.[39] Scattering from the solvent was subsequently subtracted proportionally to its volume fraction. In addition to PDMAEMA star polyelectrolytes, we also studied the solution behaviors of linear PDMAEMA with the changes of pH and temperature.

RESULTS

SANS Data Analysis Notes. As known, the SANS data from star polymers usually show two distinguishable scattering regimes, with the scattering at lower q range stems from the overall shape of the stars and intermolecular ordering, scattering at higher q value is determined by a secondary substructure, which corresponds to the intramolecular density distribution and blob structure.[40] Thus, a combination of the two appropriate models is usually required to analyze SANS experimental data in the whole q range. Spherical core−shell model provides the form factor $P(q)$ with core−shell structure (equations for this model and other models are included in the Supporting Information) and the appearance of the distinct maximum allows for the evaluation of the intermolecular distances in partially ordered solutions.[41] The intermolecular interactions can also be accounted with mean spherical approximation (MSA) approach.[42] The MSA structure factor is suitable for systems consisting of charged, spheroidal objects in a dielectric medium. When combined with the appropriate form factor (core−shell model in our case), allows the inclusion of interparticle effects due to the screened Coulomb repulsion between charged particles.[43]

The blob substructure for star polyelectrolytes needs to be analyzed with a mass fractal model (see Supporting Information). The use of the mass fractal model to parametrize scattering at higher q range in addition to a model describing the overall size of the star polymers has been reported before.[44] The mass fractal model calculates the scattering from fractal-like aggregates based on the Mildner reference.[45]

In addition to the shape-dependent model, the SANS data for PDMAEMA stars can be analyzed by the generalized Kratky analysis, which provides an additional independent way to estimate the radius of gyration of the stars by plotting $I(q)q^{1/\nu}$ vs q, where ν is the excluded volume parameter.[46] From the peak position q_{max} in Kratky plots, the radius of gyration can be calculated (see the Supporting Information for detail). The scattering from semidilute solution of linear PDMAEMA without well-defined molecular shape can be treated in terms of a hierarchical structure with two length scales: the low q-range (Debye−Anderson−Brumberger (DAB) behavior) and the high q-range (Ornstein−Zernike behavior). DAB model is used to calculate the scattering from a randomly distributed, two-phase system and gives the long-range correlation length (L), which is a measure of the average distance between contributing phases.[47] Ornstein−Zernike model gives the correlation length (ξ) of the chains,[48] which is related to the entanglement distance (blob size). The two contributions can be treated separately and added to give the total scattering intensity in the two-correlation-length model.[49]

Finally, the pair distance distribution function $p(r)$ is calculated by using a modified version of the process described by Moore et al,[50] where $I(q)$ is related to the real space $p(r)$ by Fourier transform (see Supporting Information). As is known, $p(r)$ is a histogram of all distances between point pairs within the particles weighted by the excess scattering density (which can be both positive and negative) at the points, which can be used to determine the overall shape and size of the scattering object.

PDMAEMA Stars in Semidilute Solution. First, we estimate the state of the star polyelectrolyte solutions under investigation here. According to Daoud and Cotton,[51] the overlap concentration of star polymers depends on the length of arm chain, and for relatively long arms (as is the case for all our PDMAEMA star polyelectrolytes), the overlap concentration $C^* \sim N^{-4/5}f^{2/5}\nu^{-3/5}l^{-3}$, where N is the degree of polymerization of each arm, f is the arm number, ν is the excluded volume exponent, and l is the monomer size. On the basis of this equation, all the star polyelectrolytes solution concentrations used in our SANS study are lower than C^*: the $(PDMAEMA_{170})_{18}$ concentration of 5.8 vol. % is below C^* = 7.5 vol. %, the $(PDMAEMA_{170})_{9.5}$ concentration of 4.3 vol. % is below C^* = 5.8 vol. %, and the $(PDMAEMA_{240})_{24}$ concentration of 5.6 vol. % is below C^* = 6.4 vol. %. Attempts to make estimations based on the theory for charged stars, by Rubinstein et al.,[16] were not successful because of a number of unknown parameters for systems studied here.

These calculations show that all our solutions are below concentrated solution regime without overlap of the neighboring stars that enable the study of scattering from individual star macromolecules. On the other hand, for charged polyelectrolytes the crossover from dilute to semidilute regime occurs at lower concentrations than that in solutions of neutral chains due to stronger intermolecular interactions. Therefore, all of the PDMAEMA stars in our study are in the semidilute regime with the intermolecular interactions playing an important role

and the overall the scattering originated from both form-factors of individual stars and the intermolecular interference related to the close proximity of neighboring stars.[52]

In fact, the SANS data of all PDMAEMA stars show two distinguishable scattering regimes with the broad maximum at lower q stemming from the interference between PDMAEMA stars and scattering peak at higher q due to the internal structure of individual stars (Figure 1). Such characteristic

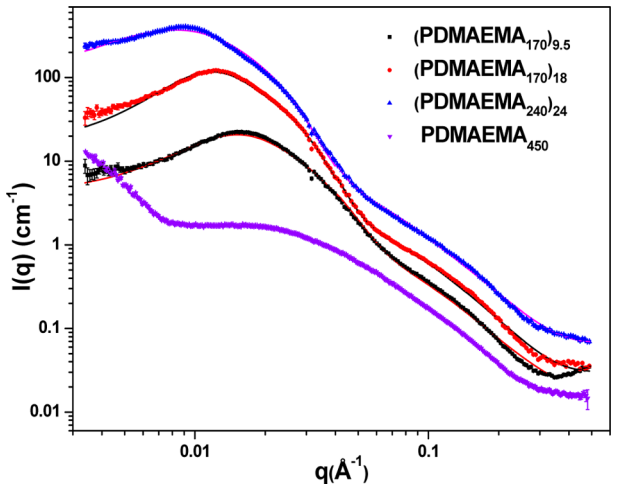

Figure 1. SANS data for solutions of PDMAEMA star polyelectrolytes with different number of arms or arm length (1 wt % at pH 7.0 and 25 °C), the solid lines are fitting with core−shell model. The curves are mutually offset by a factor of 2 for better visualization.

diffuse scattering has been reported for many polyelectrolyte systems and is attributed to the contributions from short-range ordered polyelectrolyte structures and a form-factor related to internal morphology.[53,54] In contrast, SANS for linear counterpart shows more diffuse scattering and significant intensity increase at lower q, which is characteristic of semidilute polymer solution of random coils (Figure 1).

The core−shell model combined with MSA structure factor (interparticle interference effects due to Coulomb repulsion) allows excellent fitting of the experimental data in the whole q range (Figure 1, solid lines).[43] From the MSA structure factor, the effective radius (R_{eff}) of the PDMAEMA star polymers can also be obtained (Table 1). In the case of charged spherical particles, as a consequence of the presence of the electrical double layer, the excluded volume of the particles defined by an effective radius is significantly larger than their actual radius of gyration and is responsible for large intermolecular distances as will be discussed below (Table 1).

The Kratky plots for PDMAEMA stars show a pronounced maximum, which can be used for the evaluation of the molecular dimensions under isotropic approximation (Figure 2a).[55] When $I(q)q^{1/\nu}$ vs q was plotted with a horizontal asymptotic behavior at high q range, the excluded volume parameter ν is found to be 0.6. This value for PDMAEMA stars indicates that within the blobs, the arm chains can be described as random coils in a good solvent with standard excluded volume behavior unperturbed by the interactions with other branches.[53,56] The intensity of the characteristic peak in Kratky plot increases with the increasing number of arms of PDMAEMA stars indicating more compact inner structure. The radius of gyration, R_g, can be estimated by using relationship $R_g = \sqrt{3}/q_{max}$, where q_{max} is position of the peak

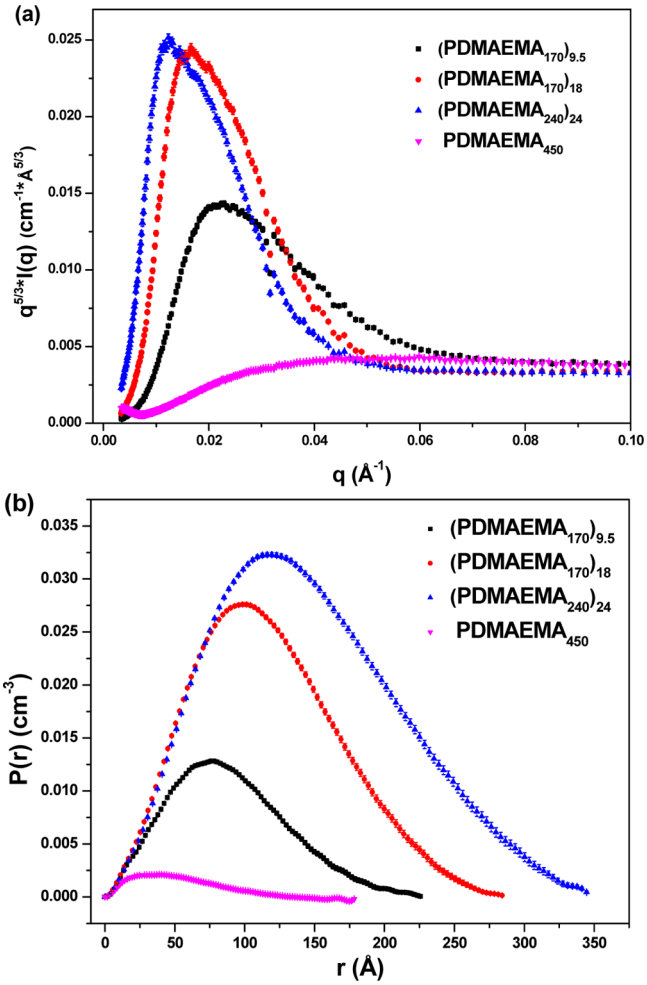

Figure 2. Kratky plots (a) and pair distance distribution functions (b) for PDMAEMA star polyelectrolytes with different number of arms or arm lengths. The data for linear $PDMAEMA_{450}$ are also shown for comparison.

at Kratky plot (Table 1, Figure 2a).[55] R_g systematically increases from 7.5 to 12.8 nm for PDMAEMA stars with increasing number of arms (or increasing molecular weight) (Table 1). For linear $PDMAEMA_{450}$ there is no obvious peak in the Kratky plot indicating random coiled state (Figure 2a).

The pair distance distribution function $p(r)$ for all stars possess symmetrical shape with correlations vanishing at the maximum distance which is defined as the effective diameter D ($D \approx 2R$ where R is defined as a peak position) (Figure 2b). The symmetrical shape of the $p(r)$ of PDMAEMA star polyelectrolytes indicates spherical structures, with the peak slightly shift to the left, indicating a denser core.[57,58] The increase of the number of arms results in the increasing correlation density and shift of the peak position to higher values (Figure 2b). The R_g obtained from the $p(r)$ peak position is in good agreement with the Kratky analysis (within standard deviation) (Table 1). The $p(r)$ analysis is not suitable for linear PDMAEMA at the same condition due to very low density variation within these scattering units.

Comparison with Theoretical Calculation. The dimensional calculations from different methods can be compared with theoretical estimations at some limiting cases (Table 2). For a star macromolecules in dilute solution with random coil

dx.doi.org/10.1021/ma500153w | Macromolecules 2014, 47, 2112−2121

Table 2. Theoretical Dimensions (nm) Estimated for PDMAEMAs under Different Assumptions

sample	R (theory)[a]	R_g (random coil)[b]	R_g (fully extended)[b]	R (uniform sphere)[c]
$(PDMAEMA_{170})_{9.5}$	12.2	8.1	17.1	5.2
$(PDMAEMA_{170})_{18}$	14.9	8.1	17.1	6.7
$(PDMAEMA_{240})_{24}$	18.3	11.2	23.9	8.2
$PDMAEMA_{450}$	–	7.2	25.1	–

[a]The theoretical radius was calculated from the equation proposed by Borisov et al.[53] [b]The R_g data were calculated based on the molecular models from Materials Studio. [c]The radius are calculated by assuming a sphere with uniform density and the same mass as PDMAEMA star.

conformation, the equation proposed by Borisov et al.[53] can be employed for the estimation of the effective dimensions:

$$R \sim aN^{\nu}p^{(1-\nu)/2}$$

where a is the monomer size, N is the degree of polymerization of each arm, p is the arm number, and ν is the scaling exponent. Two other limiting cases are random coil and fully extended conformation for all arms. The total radius of gyration of the star polymer can be evaluated by combining $2R_g$ with R_c, where R_c is the radius of the POSS core exploited for synthesis of star polyelectrolytes (around 0.75 nm) (Table 2).

Theoretical effective radii evaluated under different assumptions for star and linear chains vary in the wide range from 8 to 17 nm for the stars with the lowest molecular weight to 11 to 24 nm for the stars with the highest molecular weight (Table 2). From comparison with experimental values, it is apparent that the star dimensions with extended arms well exceed any experimental values and, thus excludes extended conformation from further consideration. On the other hand, simple random coil model for all arms does not reflect the trends observed in the experiment and, thus, should be excluded from consideration as well (Table 2). For another limiting case of a spherical particle with uniform density and the same mass as the PDMAEMA star, the calculated radius is about 67% of the experimental radius (e.g., 6.7 nm vs 10.0 nm for $(PDMAEMA_{170})_{18}$), which indicates that the stars are highly swollen and far from being densely packed spheres (Table 2). Finally, the theoretical molecular dimensions calculated considering actual star architecture constraints and random coil conformations of arms with excluded volume are still systematically (about 30%) higher than the dimensions obtained from all experimental models.

A log–log plot of experimental R_g versus M_w for PDMAEMA star polyelectrolytes is shown in Figure 3 (M_w was taken from light scattering measurements[38]). As known, the radius of gyration is expected to scale with molecular weight as $R_g = kM_w^{\nu}$, where ν is $^1/_3$ for dense homogeneous sphere and 0.6 for chains with excluded volume in a good solvent.[59,60] Our experimental data for PDMAEMA stars shows an exponent ν being close to 0.36 for all stars that again indicates the structure is close to dense but swollen spherical particles.

Overall, the analysis of all possible dimensions under different assumptions considered above indicates that neither random coil/extended distribution or simple dense spherical particles describe experimental results consistently and the estimated star dimensions in dilute solution are usually systematically than those measured experimentally (Tables 1 and 2). Therefore, an alternative model of collapsed arms with consideration of the inner structure should be used. For further analysis, we exploited a common core–shell model with a nonuniform density distribution of star polyelectrolytes as theoretically suggested for microphase-separated stars.[61]

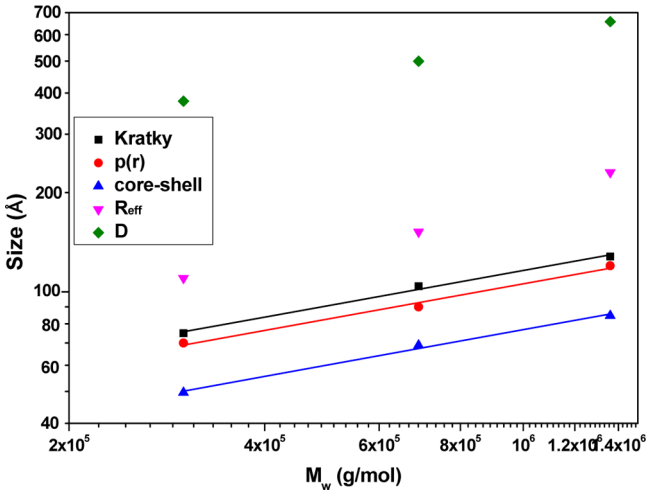

Figure 3. Characteristic dimensions versus molecular weight for PDMAEMA star polyelectrolytes. From bottom to top: R_g from core–shell model, $\nu = 0.36 \pm 0.02$; R_g from $p(r)$ analysis, $\nu = 0.35 \pm 0.03$; R_g from Kratky analysis, $\nu = 0.36 \pm 0.02$; effective radius (R_{eff}) from MSA structure factor; intermolecular distance (D) from peak position in SANS data.

Indeed, the fitting of the scattering data with core–shell model combined with MSA structural factor is applicable to all stars studied here (Figure 1). Overall, charge-corrected effective diameter of stars from this model is within 11–23 nm, which is close to the star dimensions estimated from Borisov et al[53] (Tables 1 and 2). This analysis shows that the core radius and shell thickness increase with the number of arms and arm length: core radius increases from 3.5 to 6.1 nm and the shell thickness increases from 3.7 to 6.2 nm (Table 1). The core dimensions are smaller than that estimated for fully collapsed arms (5.2–8.2 nm, Table 2) indicating the presence of significant fraction of loose chain fragments. Moreover, the mass fractal model which describes the blob substructure of the arm chains shows that the correlation length is around 1.7 nm and the excluded volume parameter of around 0.6, which again indicates the random coil structure within the blobs.

During the fitting process with core–shell model, both the core radius and shell thickness are fitting parameters, the scattering length density (SLD) of the core and shell regions is first estimated from the comparison of R_g values (Kratky analysis) with theoretical dimension as a starting value. Then, the obtained core radius and shell thickness are fixed, SLD of the core or the shell is set to be the variable to get a more accurate value, after that the radius and thickness are fitted again with the obtained SLD values to obtain the optimized dimensional parameters. The results show that SLD of the shell regions is much higher than that of core region, around 5.0×10^{-6} Å^{-2} for all PDMAEMA stars due to the presence of the D_2O with high SLD. On the other hand, SLD for cores is 1.4 ×

dx.doi.org/10.1021/ma500153w | Macromolecules 2014, 47, 2112–2121

10^{-6} Å^{-2} for $(PDMAEMA_{170})_{9.5}$ and even lower, 1.1×10^{-6} Å^{-2} for $(PDMAEMA_{170})_{18}$ and $(PDMAEMA_{240})_{24}$ stars.

Such significant difference indicates that the core region has higher concentration of polymer chains and very little solvent content as compared to the shell region with high concentration of deuterated water (Scheme 2). Such a core–shell model corresponds to quasi-micelle morphology with microphase separation of arms with loose brush-like shells and melt-like morphology of collapsed segments in dense cores due to dominating hydrophobic interactions.[61] Indeed, an estimation of the inner composition of PDMAEMA stars in the regime studied here can be based on the SLD values for bulk materials,[62] core, and shell regions. The volume fraction of solvent (deuterated water) in the core region was estimated to be around 6% further confirming dense packing of the collapsed chains. On the other hand, star shells contain up to 76% of solvent that reflects their highly swollen state (Scheme 2). Moreover, from direct comparison of chain dimensions evaluated in random coil and extended states one can conclude that chains localized in shells regions are in partially coiled, semibrush regime.

Scheme 2. Structural Changes of PDMAEMA Star Polyelectrolytes and Linear Polyelectrolytes at pH Around pK_a upon Temperature Increase[a]

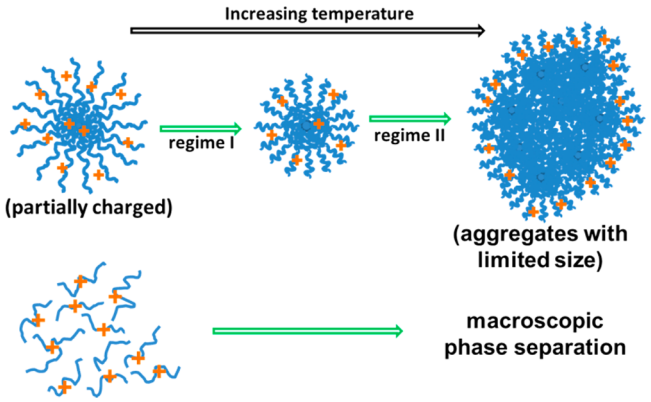

[a]For simplification, only one star macromolecule is shown before aggregation.

Finally, the presence of the broad peaks in the low q range on SANS curves of star polyelectrolytes indicates a short-range ordering of charged stars in a semidilute regime in contrast to linear PDMAEMA macromolecules (Figure 1). The formation of partially ordered stars has been observed for some star macromolecules and suggested to be controlled by long-range repulsive intermolecular interactions.[53] All peaks are very broad that corresponds to the spatial correlation expanded only over very few neighboring stars. For PDMAEMA stars with different number of arms and arm lengths, the position of the broad peak shifts to the lower q, which indicates the increasing distance between the stars (Table 1, Figure 3). Distance between stars is within 38–66 nm, which is much larger than the effective dimensions of star macromolecules (22–46 nm). These results further confirm the semidilute regime with partially collapsed individual stars interacting with each other but being far from close contact and overlap.[43]

Comparison with Fully Charged Star Polyelectrolytes. The structural differences between weak and strong star polyelectrolytes were also studied by using the quaternized ammonium salts of the PDMAEMA stars obtained by quaternization with methyl iodide.[38] In contrast to the weak star polyelectrolytes considered above, the SANS for qPDMAEMA stars show sharper peaks indicating better intermolecular ordering with significant upturn at low q (Figure 4a). The peaks are shifted to lower q indicating increased separation of star macromolecules as a result of increased repulsion (Table 1). The excessive zero-angle scattering (q < 0.08 Å^{-1}) indicates large-scale concentration fluctuations and increasing osmotic pressure within solutions of highly charged stars.[63,43]

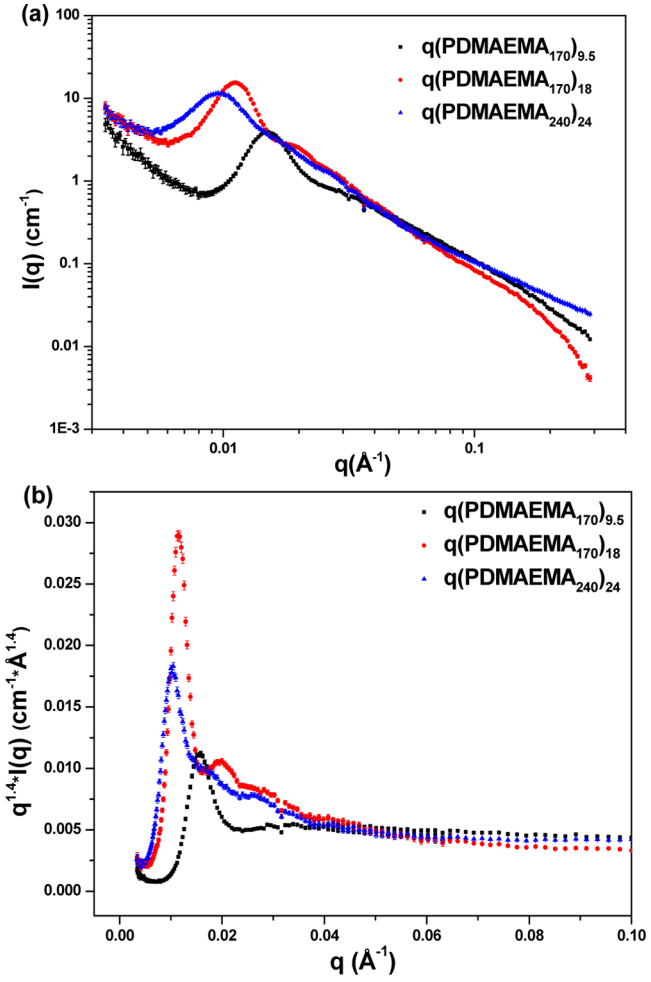

Figure 4. (a) SANS data of quaternized PDMAEMA star polyelectrolytes solution (1 wt % in D_2O) with different number of arms or arm length. (b) Kratky plot for the corresponding quaternized PDMAEMA star polyelectrolytes.

Because of expanded state of highly charged stars and higher ordering, core–shell models and pair distance distribution approach are not applicable for these solutions. Kratky analysis shows much sharper peaks, which are significantly shifted to lower q indicating increase in effective molecular dimensions along with narrowing size dispersion (Figure 4b). Moreover, the excluded volume parameter ν in Kratky plots increases to 0.7, which indicates the more expanded local blob structure due to the increasing electrostatic repulsion and osmotic pressure within the star macromolecules.[64]

Thermo-Responsiveness of PDMAEMA Star Polyelectrolytes. For further analysis of the thermo-responsive

dx.doi.org/10.1021/ma500153w | Macromolecules 2014, 47, 2112–2121

behaviors of star polyelectrolyte solutions at different pH conditions, we selected one type of star polyelectrolyte, $(PDMAEMA_{170})_{18}$, with intermediate arm length and number of arms, the pK_a of which is around 5.8.[38] At pH values close to pK_a, $(PDMAEMA_{170})^{18}$ stars are partially charged and the charge density decreases with increasing pH value. It is worth to note that at high pH conditions when the charge density is low, PDMAEMA stars show typical LCST behavior upon increasing temperature.[38] The LCST point is 31 °C at pH 9 but increases to above 80 °C for pH below 7 that is too close to the boiling point and cannot be achieved.

The SANS curves was first collected at pH 7.0, which is above the pK_a for PDMAEMA star polyelectrolytes (Figure 5a).

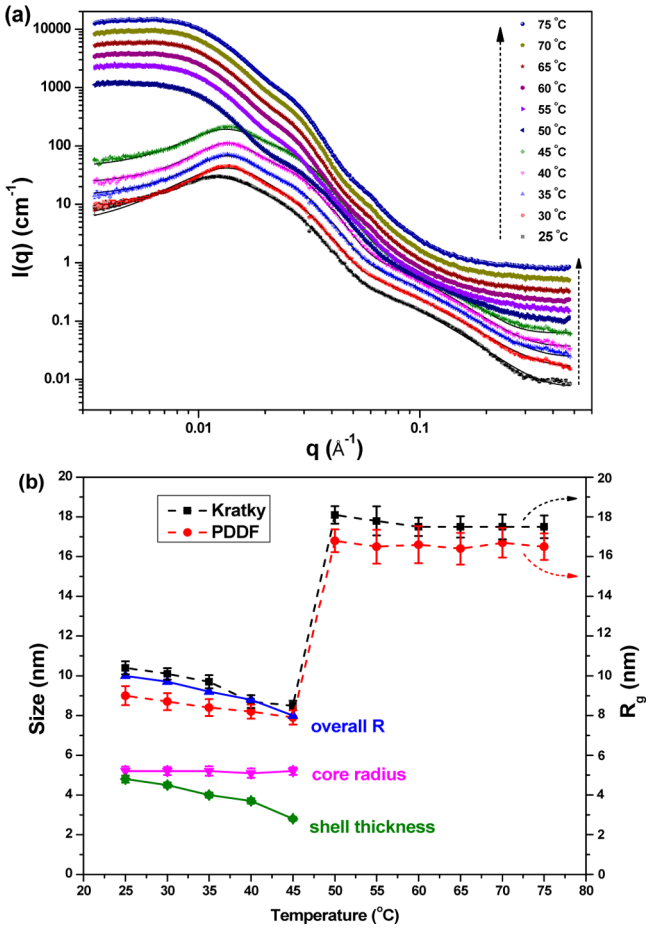

Figure 5. SANS of $(PDMAEMA_{170})_{18}$ at pH 7.0 at increasing temperature, the curves are mutually offset by a factor of 1.5 for better visualization (temperature increases from bottom to top). The solid lines (from 25 to 45 °C) represent the fitting by core−shell model. (b) Temperature dependent dimension changes from core−shell model, Kratky model and pair distance distribution functions for $(PDMAEMA_{170})_{18}$ at pH 7.0.

In the temperature range from 25 to 70 °C dramatic changes are observed. Two temperature regimes can be clearly visible: in regime I, from 25 to 45 °C, the scattering curves are similar to that obtained at room temperature with diffuse peak. However, starting from 50 °C the SANS curves changed significantly with low-q scattering dramatically increasing and shifting to lower q (Figure 5a).

Kratky analysis of scattering data and pair distance distribution in the temperature regime I show a consistent shift of the peak position toward higher q values and $p(r)$ maximum position to lower radial values (Figure S1). Therefore, in this temperature regime, R_g shows a graduate decrease by about 20% up to 45 °C (Figure 5b). Moreover, core−shell modeling also confirms the contraction of star macromolecules but additionally shows that the core size remains virtually unchanged, around 5.1 nm, while the shell gradually collapsed with the thickness decreasing by 40% from 4.8 nm to about 2.5 nm at the highest temperature of 45 °C for this regime.

In the temperature regime II (above 50 °C), the diffuse character of scattering makes it unsuitable for using the core−shell model and, thus, only Kratky plots and $p(r)$ analysis have been employed (Figure S1). These analyses show that the R$_g$ increases significantly from 8.5 nm at 45 °C to 18.1 nm at 50 °C within very narrow temperature range, and remains virtually unchanged at even higher temperatures (Figure 5b). Such dramatic and sharp change in the characteristic molecular dimensions can be associated with intramolecular microphase separation, as will be discussed later.

SANS measurements were also conducted at pH 5.5, which is slightly below pK_a, so that the star polyelectrolytes are charged to a higher extent. Similarly to the pH 7 condition discussed above, two distinct temperature regimes are observed in the temperature range from 25 to 50 °C and from 55 to 75 °C (Figure 6a).

Similarly, Kratky and $p(r)$ analysis (Figure S2) show a consistent decrease in R$_g$ with temperature within the first regime, with the core dimensions remain almost constant, around 5.3 nm, and shell gradually collapses by about 30% (Figure 6b). Furthermore, at temperatures above 55 °C, the R_g increases by 50%, to 12.2 nm within narrow temperature interval, and then remains virtually constant at higher temperatures (Figure 6b). Overall, the transition temperature is slightly shifted to higher temperature and dimensional changes are less dramatic at lower pH.

Comparison Star and Linear PDMAEMA Polyelectrolytes. Finally, we conducted comparative study of linear PDMAEMA at the same concentration, temperature range, and pH conditions (Figure 7).

At both pH values studied here, a broad diffuse scattering in the intermediate q range and increasing scattering intensity at lower q are observed. When the temperature increases to 45 °C and above, a significant increase in scattering intensity is observed at low q. Fitting of the scattering data for linear PDMAEMA was conducted with Ornstein−Zernike model that gives the short-range correlation length, ξ, of around 1.7 nm at 25 °C with modest variation in a whole temperature range (1.7 nm −2.4 nm) (Figure S3). This is close to the characteristic dimensions of blobs in solutions of star polymers.[43] On the other hand, the DAB model which is applicable here only to SANS curves at elevated temperatures and low q range, gives the long-range correlation length L of above 100 nm (at pH 7.0 condition) at 45 °C which further increases at higher temperature and achieves the limit of resolution in this study (Figure S3). The results at lower pH condition (pH 5.5) show similar trends with smaller absolute values (Figure S3).

GENERAL DISCUSSION AND CONCLUSIONS

Before general discussion it is worth to note that PDMAEMA polyelectrolytes at pH 5.5, which is slightly lower than the pK_a, are more charged than at pH 7.0. In addition, since the use of buffer is detrimental in a salt-free system,[38] the pH value in the

dx.doi.org/10.1021/ma500153w | Macromolecules 2014, 47, 2112−2121

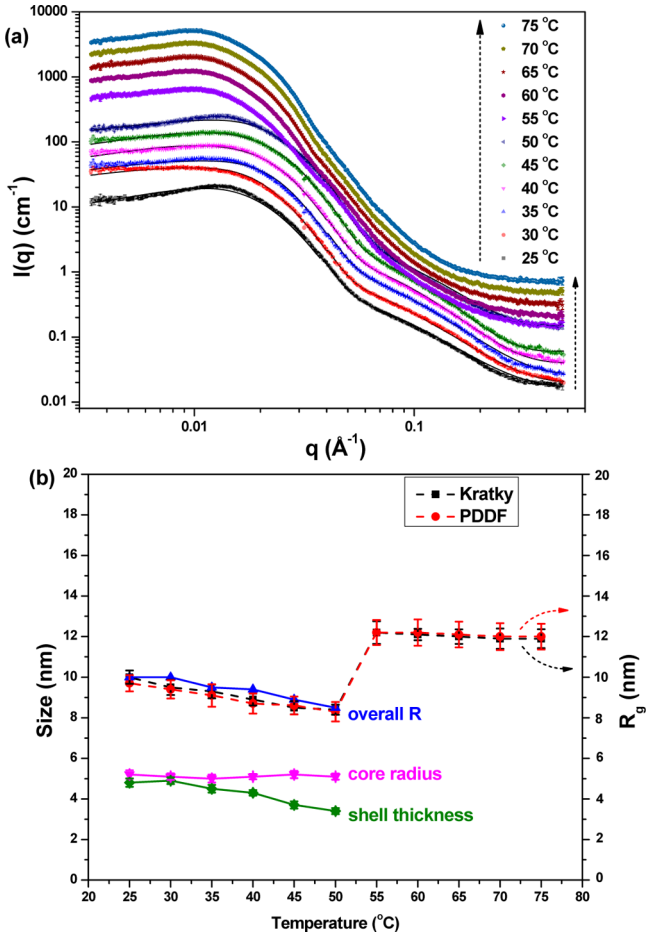

Figure 6. (a) SANS data of $(PDMAEMA_{170})_{18}$ at pH 5.5 with increasing temperature, the curves are mutually offset by a factor of 1.5 for better visualization (temperature increases from bottom to top). The solid lines (from 25 to 50 °C) represent the fitting by core−shell model. (b) Temperature dependent dimension changes from core−shell model, Kratky model and pair distance distribution functions for $(PDMAEMA_{170})_{18}$ at pH 5.5.

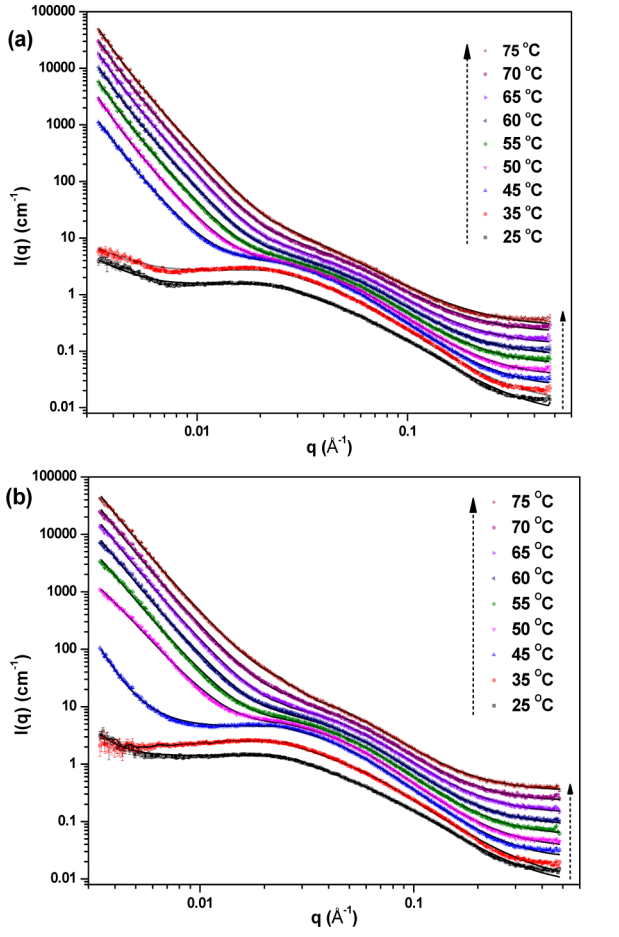

Figure 7. SANS data of $PDMAEMA_{450}$ at pH 7.0 (a) and pH 5.5 (b) with increasing temperature, the curves are mutually offset by a factor of 1.5 for better visualization (temperature increases from bottom to top). The solid lines are from the combined Ornstein−Zernike and DAB model fittings.

salt free solution decreases with increasing temperature (e.g., from 7.0 at 25 °C to 5.7 at 75 °C, Figure S4), which also plays a role in the observed phenomena. Moreover, the pH vs temperature curves for $(PDMAEMA_{170})_{18}$ solution shows a kink at around 50 °C, which is close to the transition temperatures between regimes I and II detected in this study. The pH dependence with temperature of PDMAEMA stars with different number of arms in dilute water solution has similar characters (Figure S5).[65]

The results of the dimensional changes for PDMAEMA star polyelectrolytes in semidilute solution can be understood in terms of local variations of the balance between intermolecular and intramolecular interactions. General schematics of molecular transformations suggested in this study for star polyelectrolytes are presented in Scheme 2. First, we suggest that at room temperature, star macromolecules in semidilute solution possess core−shell morphology with higher density collapsed cores and less dense shells composed of highly swollen arms as discussed before. In the temperature regime I, the arm chains gradually collapse mainly due to the decrease in the osmotic pressure within stars and the decrease of solvent quality with increasing temperature. Indeed, it has been demonstrated that in semidilute solution, temperature increase results in the decreasing concentration of confined couterions and thus, the osmotic pressure decreases within the stars.[66] Moreover, with the increase of temperature, the pH value of PDMAEMA solution slightly decreases that causes the star macromolecules becoming more deprotonated and certain amount of protons are released to the solution. As a result, the charge density of arm chains decreases to a certain extent, which also contributes to the decreased electrostatic repulsion and increased hydrophobic interactions that promotes arm collapse in the outer shells.

At a certain temperature, the sudden transition to a regime dominated by hydrophobic interactions occurs which results in the formation of limited intermolecular aggregates (aggregation number below 10, similar to theoretical estimation[67]) (Scheme 2). During this sharp transition, the strong screening of charges and the increased hydrophobic interaction as well as the attractive force between ion pairs synergistically lead to the limited intermolecular aggregation of neighboring stars. Moreover, the partially charged PDMAEMA star polyelectrolytes contain annealed charges, which can more from one repeat unit to another in an optimum way so that to minimize the loss in translational entropy of the counterions.[23] The annealed charge redistribution results in the microphase intramolecular separation with the formation of hydrophobic clusters consisting of several densely packed hydrophobic domains

dx.doi.org/10.1021/ma500153w | Macromolecules 2014, 47, 2112−2121

surrounded by charged hydrophilic regions swollen by solvent. Such limited-aggregated structures facilitate their stability upon further increase in temperature without macroscopic phase separation,[68] similarly to that observed for amphiphilic polyelectrolyte hydrogels.[69] The screening of charges by increased counterion condensation and hydrophobic interactions can be considered as the main causes for such aggregation in this temperature regime. The compact structure of star polyelectrolytes provides strong steric repulsion, which effectively prevents large-scale aggregation due to the intermolecular interactions. No macroscopic phase separation occurs and a real LCST is out-of-reach according to previous studies but the observed limited aggregation can be considered as "pre-transitional" behavior below the phase boundary.[38]

Finally, the effect of pH on the state of PDMAEMA star polyelectrolyte solutions has been revealed in this study as well. Indeed, the size of intramolecular aggregates decreases at pH 5.5 condition due to the stronger electrostatic repulsion, the transition temperature for the microphase separation also increases, and the aggregation number decreases from 10 at pH 7.0 to around 3 at pH 5.5. In contrast, the temperature behavior of solution of linear PDMAEMA polyelectrolytes is very different from that of star PDMAEMA. The high scattering intensity at low-q indicates the presence of large-scale inhomogeneities observed for semidilute polyelectrolyte solutions.[70] Significant increase in this scattering at low q range at elevated temperature indicates large-scale phase separation, which has been further proven by DAB model analysis. As a result, linear PDMAEMA solutions exhibit conventional macroscopic condensation caused by dominating hydrophobic interactions in contrast to core−shell star polyelectrolytes under the same conditions (Scheme 2).

The structural behavior observed here are underpinned by recent studies, which show that the conformation of polyelectrolyte stars in aqueous solution is controlled by hydrophobic interactions, which promote a collapse of the arms, while the electrostatic forces lead to a swelling of the chains in outer loose shells.[61] In a semidilute PDMAEMA star polyelectrolyte solution, electrostatic repulsion results in the partially collapsed arm chains and the size of stars is also smaller compared with that in dilute solution.[36] Moreover, salt- and buffer-free solutions provide negligible electrostatic screening that might further explain the absence of a phase boundary for PDMAEMA star polyelectrolyte in pure water solution at 0.1 g/L within the experimental window (20−80 °C).[38]

Indeed, polyelectrolyte brushes possess smaller dimensions at increasing concentration due to the increased counterion adsorption and/or Donnan salt partitioning between the coronal layer and the surrounding medium.[24] Simulations showed that for strongly charged polyelectrolyte chains under poor solvent condition in a salt-free solution, the polyelectrolyte concentration plays a vital role in the balance between electrostatic and hydrophobic interactions.[71,72] At low polymer concentration, the polyelectrolyte chains form necklaces of beads connected by strings as solvent quality decreases. At high polyelectrolyte density there is a crossover from dominating electrostatic interaction to a regime where the hydrophobic interactions dominate because of the electrostatic interactions are screened on length scales larger than the correlation length.

The effects of increasing temperature (or decrease of solvent quality) on star polymers were reported, which result in coil-to-globule transition or shrinkage of the stars.[36,73] Moreover, a molecular dynamics study of polyelectrolyte stars showed that the R_g value consistently decreases with decreasing solvent quality.[74] Another study[66] showed that if the Coulomb interaction strength exceeds a critical value, counterions condense on the chain and ion pairs are formed, so that the charges on the chains are largely screened and the ion pairs also possess a net attraction.[75] The counterion condensation leads to inhomogeneous charge redistribution, and the resulting attractive interaction leads to the collapse of polyelectrolyte chains and eventually to the formation of intermolecular aggregates.

■ ASSOCIATED CONTENT

Supporting Information

Detailed description of the models used to fit the SANS data. This material is available free of charge via the Internet at http://pubs.acs.org/.

■ AUTHOR INFORMATION

Corresponding Author

*(V.V.T.) E-mail: vladimir@mse.gatech.edu.

Present Address

[‖]Institut für Organische Chemie, Johannes Gutenberg-Universität Mainz, D-55099 Mainz, Germany.

Notes

The authors declare no competing financial interest.

■ ACKNOWLEDGMENTS

This work is supported by the NSF-DMR 1002810 grant. The authors are grateful to S. Malak for discussion and technical assistance. C. V. Synatschke acknowledges funding through a BayEFG scholarship and support from the Elite Network of Bavaria. SANS experiments at Oak Ridge National Laboratory's High Flux Isotope Reactor are supported by the Scientific User Facilities Division, Office of Basic Energy Sciences, U.S. Department of Energy.

■ REFERENCES

(1) Mei, Y.; Lauterbach, K.; Hoffmann, M.; Borisov, O. V.; Ballauff, M.; Jusufi, A. *Phys. Rev. Lett.* **2006**, *97*, 158301−158304.

(2) Schuh, C.; Santer, S.; Prucker, O.; Rühe, J. *Adv. Mater.* **2009**, *21*, 1−5.

(3) Ramzi, A.; Scherrenberg, R.; Joosten, J.; Lemstra, P.; Mortensen, K. *Macromolecules* **2002**, *35*, 827−833.

(4) Liu, X.; Cheng, F.; Liu, H.; Chen, Y. *Soft Matter* **2008**, *4*, 1991−1994.

(5) Peleshanko, S.; Gunawidjaja, R.; Petrash, S.; Tsukruk, V. V. *Macromolecules* **2006**, *39*, 4756−4766.

(6) Plamper, F. A.; Reinicke, S.; Elomaa, M.; Schmalz, H.; Tenhu, H. *Macromolecules* **2010**, *43*, 2190−2203.

(7) Jusufi, A.; Likos, C. N. *Rev. Mod. Phys.* **2009**, *81*, 1753−1772.

(8) Steinschulte, A.; Schulte, B.; Drude, N.; Erberich, M.; Herbert, C.; Okuda, J.; Möller, M.; Plamper, F. A. *Polym. Chem.* **2013**, *4*, 3885−3895.

(9) Peleshanko, S.; Gunawidjaja, R.; Jeong, J.; Shevchenko, V. V.; Tsukruk, V. V. *Langmuir* **2004**, *20*, 9423−9427.

(10) Gunawidjaja, R.; Peleshanko, S.; Genson, K. L.; Tsitsilianis, C.; Tsukruk, V. V. *Langmuir* **2006**, *22*, 6168−6176.

(11) Gunawidjaja, R.; Peleshanko, S.; Tsukruk, V. V. *Macromolecules* **2005**, *38*, 8765−8774.

(12) Peleshanko, S.; Tsukruk, V. V. *Prog. Polym. Sci.* **2008**, *33*, 523−580.

(13) Peleshanko, S.; Tsukruk, V. V. *J. Polym. Sci., Part B: Polym. Phys.* **2012**, *50*, 83−100.

(14) Stuart, M. C.; Huck, W.; Genzer, J.; Müller, M.; Ober, C.; Stamm, M.; Sukhorukov, G.; Szleifer, I.; Tsukruk, V. V.; Urban, M.;

Winnik, F.; Zauscher, S.; Luzinov, I.; Minko, S. *Nat. Mater.* **2010**, *9*, 101−113.
(15) Plamper, F. A.; Gelissen, A. P.; Timper, J.; Wolf, A.; Zezin, A. B.; Richtering, W.; Tenhu, H.; Simon, U.; Mayer, J.; Borisov, O. V.; Pergushov, D. V. *Macromol. Rapid Commun.* **2013**, *34*, 855−860.
(16) Dobrynin, A. V.; Rubinstein, M. *Prog. Polym. Sci.* **2005**, *30*, 1049−1118.
(17) Boudou, T.; Crouzier, T.; Ren, K.; Blin, G.; Picart, C. *Adv. Mater.* **2010**, *22*, 441−467.
(18) Kanai, S.; Muthukumar, M. *J. Chem. Phys.* **2007**, *127*, 244908.
(19) Muthukumar, M.; Hua, J.; Kundagrami, A. *J. Chem. Phys.* **2010**, *132*, 084901.
(20) Verso, F. L.; Likos, C. N.; Reatto, L. *Prog. Colloid Polym. Sci.* **2006**, *133*, 78−87.
(21) Borue, V. Y.; Erukhimovich, I. Y. *Macromolecules* **1988**, *21*, 3240−3249.
(22) Prabhu, V. M.; Muthukumar, M.; Wignall, G. D.; Melnichenko, Y. B. *J. Chem. Phys.* **2003**, *119*, 4085−4098.
(23) Bokias, G.; Vasilevskaya, V. V.; Iliopoulos, I.; Hourdet, D.; Khokhlov, A. R. *Macromolecules* **2000**, *33*, 9757−9763.
(24) Korobko, A. V.; Jesse, W.; Egelhaaf, S. U.; Lapp, A.; van der Maarel, J. R. C. *Phys. Rev. Lett.* **2004**, *93*, 177801.
(25) Adelsberger, J.; Grillo, I.; Kulkarni, A.; Sharp, M.; Bivigou-Koumba, A. M.; Laschewsky, A.; Muller-Buschbaum, P.; Papadakis, C. M. *Soft Matter* **2013**, *9*, 1685−1699.
(26) Xu, W.; Choi, I.; Plamper, F. A.; Synatschke, C. V.; Müller, A. H. E.; Tsukruk, V. V. *ACS Nano* **2013**, *7*, 598−613.
(27) Choi, I.; Malak, S. T.; Xu, W.; Heller, W. T.; Tsitsilianis, C.; Tsukruk, V. V. *Macromolecules* **2013**, *46*, 1425−1436.
(28) Choi, I.; Suntivich, R.; Plamper, F. A.; Synatschke, C. V.; Müller, A. H. E.; Tsukruk, V. V. *J. Am. Chem. Soc.* **2011**, *133*, 9592−9606.
(29) Schallon, A.; Synatschke, C. V.; Jérôme, V.; Müller, A. H. E.; Freitag, R. *Biomacromolecules* **2012**, *13*, 3463−3474.
(30) Luzinov, I.; Minko, S.; Tsukruk, V. V. *Prog. Polym. Sci.* **2004**, *29*, 635−698.
(31) Griffiths, P. C.; Alexander, C.; Nilmini, R.; Pennadam, S. S.; King, S. M.; Heenan, R. K. *Biomacromolecules* **2008**, *9*, 1170−1178.
(32) Shibayama, M.; Tanaka, T.; Han, C. C. *J. Chem. Phys.* **1992**, *97*, 6829−6841.
(33) Stieger, M.; Richtering, W.; Pedersen, J. S.; Lindner, P. *J. Chem. Phys.* **2004**, *120*, 6197−6206.
(34) Ramzi, A.; Rijcken, C. J.; Veldhuis, T. F.; Schwahn, D.; Hennink, W. E.; van Nostrum, C. F. *J. Phys. Chem. B* **2008**, *112*, 784−792.
(35) He, L.; Cheng, G.; Melnichenko, Y. B. *Phys. Rev. Lett.* **2012**, *109*, 067801.
(36) Lambeth, R. H.; Ramakrishnan, S.; Mueller, R.; Poziemski, J. P.; Miguel, G. S.; Markoski, L. J.; Zukoski, C. F.; Moore, J. S. *Langmuir* **2006**, *22*, 6352−6360.
(37) Plamper, F. A.; Schmalz, A.; Penott-Chang, E.; Drechsler, M.; Jusufi, A.; Ballauff, M.; Mueller, A. H. E. *Macromolecules* **2007**, *40*, 5689−5697.
(38) Plamper, F. A.; Ruppel, M.; Schmalz, A.; Borisov, O.; Ballauff, M.; Mueller, A. H. E. *Macromolecules* **2007**, *40*, 8361−8366.
(39) Cheng, G.; Melnichenko, Y. B.; Wignall, G. D.; Hua, F. J.; Hong, K.; Mays, J. W. *Macromolecules* **2008**, *41*, 9831−9836.
(40) Rathgeber, S.; Gast, A. P.; Hedrick, J. L. *Appl. Phys. A: Mater. Sci. Process* **2002**, *74*, s396−s398.
(41) Guinier, A.; Fournet, G. *Small-Angle Scattering of X-Rays*; John Wiley and Sons: New York, 1955.
(42) Hansen, J. P.; Hayter, J. B. *Mol. Phys.* **1982**, *46*, 651−656.
(43) Richter, D.; Jucknischke, O.; Willner, L.; Fetiers, L. J.; Lin, M.; Huang, J. S.; J. Roovers, J.; Toporovski, C.; Zhou, L. L. *J. Phys. IV* **1993**, *3*, 3−12.
(44) Likos, C. N.; Lowen, H.; Poppe, A.; Willner, L.; Roovers, J.; Cubitt, B.; Richter, D. *Phys. Rev. E: Stat., Nonlinear, Soft Matter Phys.* **1998**, *58*, 6299−6307.
(45) Mildner, D.; Hall, P. *J. Phys. D: Appl. Phys.* **1986**, *19*, 1535−1545.
(46) Crawford, M. K.; Smallew, R. J.; Cogen, G.; Hogan, B.; Wood, B.; Kumar, S. K.; Melnichenko, Y. B.; He, L.; Guise, W.; Hammouoda, B. *Phys. Rev. Lett.* **2013**, *110*, 196001.
(47) Debye, P.; Anderson, H. R.; Brumberger, H. *J. Appl. Phys.* **1957**, *28*, 679−683.
(48) De Gennes, P. G. *Scaling concepts in polymer physics*; Cornell University Press: Ithaca, NY, 1979.
(49) Hammouda, B.; Ho, D.; Kline, S. *Macromolecules* **2002**, *35*, 8578−8585.
(50) Moore, P. B. *J. Appl. Crystallogr.* **1980**, *13*, 168−175.
(51) Daoud, M.; Cotton, J. P. *J. Phys. (Paris)* **1982**, *43*, 531−538.
(52) Dozier, W. D.; Huang, J. S.; Fetters, L. J. *Macromolecules* **1991**, *24*, 2810−2814.
(53) Borisov, O. V.; Zhulina, E. B.; Leermakers, F. A. M.; Ballauff, M.; Müller, A. H. E. *Adv. Polym. Sci.* **2011**, *241*, 1−55.
(54) Kjøniksen, A. L.; Zhu, K.; Behrens, M. A.; Pedersen, J. S.; Nyström, B. *J. Chem. Phys. B* **2011**, *115*, 2125−2139.
(55) Hedden, R. C.; Bauer, B. J. *Macromolecules* **2003**, *36*, 1829−1835.
(56) Hammouda, B. *Macromol. Theory Simul.* **2012**, *21*, 372−381.
(57) Yun, S. I.; Lai, K.; Briber, R. M.; Teertstra, S. J.; Gauthier, M.; Bauer, B. J. *Macromolecules* **2008**, *41*, 175−183.
(58) Rathgeber, S.; Monkenbusch, M.; Kreitschmann, M.; Urban, V.; Brulet, A. *J. Chem. Phys.* **2002**, *117*, 4047−4062.
(59) Yun, S. I.; Briber, R. M.; Kee, R. A.; Gauthier, M. *Polymer* **2003**, *44*, 6579−6587.
(60) Sperling, L. H. *Introduction to Physical Polymer Science*; John Wiley & Sons, Inc., Hoboken, NJ, 2006.
(61) Rud, O. V.; Mercurieva, A. A.; Leermakers, F. A. M.; Birshtein, T. M. *Macromolecules* **2012**, *45*, 2145−2160.
(62) An, S. W.; Su, T. J.; Thomas, R. K.; Baines, F. L.; Billingham, N. C.; Armes, S. P.; Penfold, J. *J. Phys. Chem. B* **1998**, *102*, 387−393.
(63) Wang, D.; Moses, D.; Bazan, G. C.; Heeger, A. J.; Lal, J. *J. Macromol. Sci., Part A: Pure Appl. Chem.* **2001**, *38*, 1175−1189.
(64) Hsu, H.; Paul, W.; Binder, K. *J. Chem. Phys.* **2012**, *137*, 174902.
(65) Plamper, F. *Star shaped polyelectrolytes*; University of Bayreuth: Bayreuth, Germany, 2007.
(66) Khalatur, P. G.; Khokhlov, A. R.; Mologin, D. A.; Reineker, P. *J. Chem. Phys.* **2003**, *119*, 1232−1247.
(67) Stradner, A.; Sedgwick, H.; Cardinaux, F.; Poon, W. C.; Egelhaaf, S. U.; Schurtenberger, P. *Nature* **2004**, *432*, 492−495.
(68) Mai, Y.; Eisenberg, A. *Chem. Soc. Rev.* **2012**, *41*, 5969−5985.
(69) Andreeva, A. S.; Philippova, O. E.; Khokhlov, A. R.; Islamov, A. K.; Kuklin, A. I. *Langmuir* **2005**, *21*, 1216−1222.
(70) Ermi, B. D.; Amis, E. J. *Macromolecules* **1998**, *31*, 7378−7384.
(71) Micka, U.; Holm, C.; Kremer, K. *Langmuir* **1999**, *15*, 4033−4044.
(72) Micka, U.; Kremer, K. *Europhys. Lett.* **2000**, *49*, 189−195.
(73) Huissmann, S.; Blaak, R.; Likos, C. N. *Macromolecules* **2009**, *42*, 2806−2816.
(74) Košovan, P.; Kuldová, J.; Limpouchová, Z.; Procházka, K.; Zhulina, E. B.; Borisov, O. V. *Soft Matter* **2010**, *6*, 1872−1874.
(75) Winkler, R. G.; Gold, M.; Reineker, P. *Phys. Rev. Lett.* **1998**, *80*, 3731−3734.